Physics of Fluids

Independent friction-restitution modeling of two-disk collisions

Cite as: Phys. Fluids **33**, 043305 (2021); https://doi.org/10.1063/5.0044963
Submitted: 21 January 2021 . Accepted: 12 March 2021 . Published Online: 07 April 2021

Antonio Doménech-Carbó, Elena Montagna, and María Teresa Doménech-Carbó

View Online Export Citation CrossMark

Physics of Fluids
SPECIAL TOPIC: Tribute to
Frank M. White on his 88th Anniversary
SUBMIT TODAY!

AIP Publishing

© 2021 Author(s).

Physics of Fluids ARTICLE scitation.org/journal/phf

Independent friction-restitution modeling of two-disk collisions

Cite as: Phys. Fluids **33**, 043305 (2021); doi: 10.1063/5.0044963
Submitted: 21 January 2021 · Accepted: 12 March 2021 ·
Published Online: 7 April 2021

View Online Export Citation CrossMark

Antonio Doménech-Carbó,[1,a)] Elena Montagna,[2] and María Teresa Doménech-Carbó[2]

AFFILIATIONS

[1]Department of Analytical Chemistry, University of Valencia, Dr. Moliner 50, 46100 Burjassot (València), Spain
[2]Departament de Conservació i Restauració de Bens Culturals/Institut de Restauració del Patrimoni, Universitat Politécnica de València, Camí de Vera 14, 46022 València, Spain

[a)]Author to whom correspondence should be addressed: antonio.domenech@uv.es

ABSTRACT

The oblique collisions between two axisymmetric disks moving on a flat horizontal surface are described in terms of impact modeling based on the assumption that normal and tangential restitution mechanisms operate independently of friction. Describing these mechanisms in terms of the usual Coulomb formulation, the model allows for an interpretation of some "anomalous" experimental data reported in the literature. These experimental data, corresponding to the variation of the coefficients of friction and tangential restitution with the impact angle, remained unexplained in classic formulations, are understood within the framework of the independent friction-restitution closure. Experimental data for metallic coins are in agreement with that formulation, including rolling friction effects.

Published under license by AIP Publishing. https://doi.org/10.1063/5.0044963

I. INTRODUCTION

Collisions are extensively treated in the mechanics literature dealing with fluid mechanics,[1–6] granular matter,[7–9] and aerosol science,[10,11] among other fields. Much of this research is focused on the impact of spheres on surfaces[12–17] and two-sphere collisions.[18–20] More recently, the description of collisions between particles and fluid/wall collisions is receiving attention because of the difficulty to describe out-of-equilibrium situations[21,22] and the determination of flow velocity in deflected nanotubes.[23] In this context, several studies have evidenced the interest of disk collisions in fluid mechanics.[24,25]

These phenomena are described using two general approaches: in smooth or continuous modeling, the impact event is described in terms of forces acting during a finite time in a small region where the contact between the bodies occurs (the contacting points); in nonsmooth or discontinuous modeling, the impact is described in terms of instantaneous impulses determining abrupt changes in the linear and angular momentums of the colliding bodies.[26,27] Real, inelastic impacts are governed by the laws of conservation of linear and angular momentums, but significant energy is involved in elastoplastic deformations, vibrations, and wave propagation. In the following, these last energy terms will be neglected, as is customary in the abundant literature on impact under predominating elastoplastic contact at moderate velocities.[28–35]

There is abundant experimental evidence supporting the idea that the impact between rigid bodies involves at least two different dynamic regimes. In a sliding collision, the tangential components of precollision and postcollision relative velocities at the contact point are both nonzero and projected in the same direction. Such collisions are termed as sliding,[28–31] gross sliding collisions,[32] continuous sliding,[33] persistent sliding,[34] or fully sliding.[35] The collisions where the above condition does not apply are termed as no-sliding,[29] partially sliding,[35] rolling,[28] nonpersistent sliding,[34] noncontinuous sliding,[33] or sticking collisions.[31] In the following, we will use the terms sliding and sticking to identify these impact regimes.

In the discontinuous modeling of collisions, the information of the impact events is obtained from Newton's equations providing that the geometry and impulses are known. These impulses, however, have to be defined independently from Newton's equations. The first level of description is based on the use of the coefficients of restitution (normal and tangential) and friction. These are phenomenological coefficients, assumed—in principle—to be independent of the incoming velocity and impact angle and only dependent on the materials of the bodies. The view of these coefficients as "constants," however, is a rough approximation that can only be considered as reasonably valid under conditions of low-velocity impact without adhesive and/or viscous effects.[36,37]

Published under license by AIP Publishing

Two aspects have been unanimously treated in the literature on collisions under moderate impact velocities and elastoplastic contact between rigid bodies where energy losses are expressed in terms of restitution and friction.[26–40] The first one is the expression of normal impulses in terms of the coefficient of normal restitution, e_n. Although dynamic definitions are possible,[26] it is in general kinematically defined as the negative ratio of the postimpact to preimpact normal components of the relative velocity of the contacting points of the colliding bodies[27,28,33,38–40] (or equivalently, in terms of the center-of-mass velocities).[8,34,41–43] The second one is the description of impact in sliding regime on the basis of Coulomb friction laws assuming that the tangential impulse to normal impulse ratio in an oblique, two-dimensional sliding collision is equal to the coefficient of (kinetic) friction.[28–31]

To describe the stick regime of impact, however, there are a variety of approaches. In the models of Brach[29] and Kane and Levinson,[30] it is assumed that the tangential relative velocity of the contact point of the colliding bodies is zero just after the impact. This condition, however, is contradicted by experimental data revealing that, in sticking collisions, there is a reversal of such relative tangential velocity.[28,33–35,38–43]

This difficulty is solved by Walton's model[38] in which the collisions in sticking regime are described in terms of the coefficient of tangential restitution, e_t. Here, we will adopt the definition of this coefficient as the negative ratio of the postcollision to precollision tangential components of the relative velocity of the contacting points of the bodies.[38–40] Although this model shows, in general, a satisfactory agreement with experimental data, it does not capture, as emphasized by Calsamiglia *et al.*,[35] that entire range of impact angles with a single value of e_t[8,39–43] and is unable to justify several "anomalous" experimental results reported by Louge *et al.*[39,40,44] and Chatterjee *et al.*[35,45] The same difficulties appear for continuous–discontinuous models considering contact force models ultimately inspired by the Hertz's contact theory.[28,32,41,42,46–56] In these models, Young's modulus and the Poisson's coefficient enter in the motion equations. These formulations, although agree with experimental data, offer several problems underlined by Kim and Dunn[10] and Thornton *et al.*:[54,55] (i) they provide semianalytical solutions of the equations of motion; (ii) involve the use of an adjustable parameter, the tangential to normal stiffnesses; (iii) require that some adjustable physical parameters (Young's modulus and Poisson's coefficient) have to be known *a priori*, i.e., from experiments independent of the impact event.

In this context, an alternative model was proposed within the level of significance of this type of formulations, assuming that the restitution and friction effects operate independently and simultaneously in all impact regimes.[57–59] This closure involves the redefinition of normal restitution and tangential restitution as the aforementioned velocity ratios *in the absence of frictional effects*. In turn, friction is formulated on the basis of the Coulombs laws as acting *in the absence of tangential restitution effects*. As a result, the independent friction-restitution modeling (IFR) yields analytical solutions of the motion equations using a unique set of values of the coefficients of normal restitution, tangential restitution, and friction regardless of the impact of angle values. Application of this closure to the impact of spheres and disks on infinitely massive rough planes provided a satisfactory agreement with experimental data in the literature[10,11,28,31,33–35,39–47] for macrospheres[58,59] and microspheres,[60] admitting the refinement by incorporating rolling friction effects,[61] in line with Iwashita and Oda[62] and Orlando and Shen.[63] In particular, the IFR formulation permits to interpret several of the previously mentioned "anomalous" experimental data[35,39,40,44,45] now becoming as "ordinary" behavior predicted by the model.

The purpose of the current work is (i) to extend the IFR model previously applied to the rebound of spheres on massive planes, to two-body collisions, taking two axisymmetric disks, one of which being initially at rest, moving on a flat horizontal surface (ii) discuss the effect of arbitrary masses and initial rotation to describe the post-impact parameters; (iii) compare the predictions of the IFR model with classic impact ones; (iv) discuss the influence of rolling friction effects. As a result, the postcollision linear and angular velocities can be expressed as a function of the precollision ones as well as velocity-independent relationships between the angles of impact and scattering, able to be experimentally tested. This formulation improves those previously reported for the collisions of disks[64] based on Brach's model.[29] Consideration of the translational and rotational motions of disks on surfaces[25,65] permits to propose additional testable relationships. Experimental data for the collisions of different pairs of disks on rough surfaces were obtained using a conventional photographic-assisted arrangement.[64]

II. THEORY

A. General aspects

Let us consider the oblique impact of an axisymmetric disk, of mass m_1 and radius R_1, moving on a horizontal, flat surface, on a second homogenous disk of mass m_2 and radius R_2, which is initially at rest, as schematically represented in Fig. 1. A normal-tangential coordinate system will be used, the normal axis connecting the disk's centers at the collision, and the tangential axis being perpendicular to the above.

The motion equations are governed by the laws of conservation of linear and angular momentum whereas energy is not conserved. In order to establish explicit relationships between the factors (restitution and friction, *vide infra*) influencing energy losses, it will be assumed

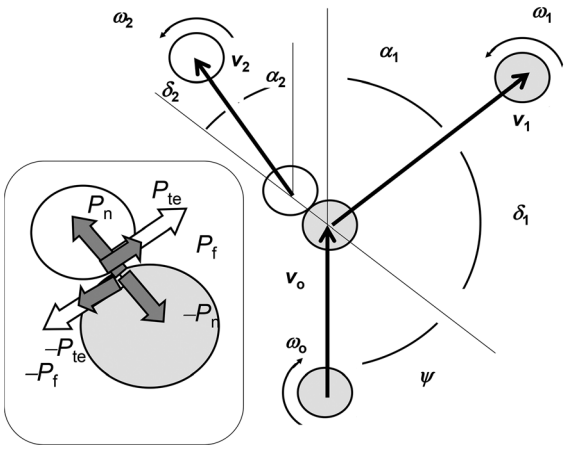

FIG. 1. Scheme for the oblique impact between axisymmetric disks moving on a horizontal, flat surface. Inset: Diagram for the impulses acting on disks 1 and 2 during the impact event.

Published under license by AIP Publishing

that, during the "instantaneous" impact event, tangential and normal impulses, P_t, P_n, act on the disks. Such linear impulses can be related to the tangential and normal components (denoted in the following by the subscripts t, n) of the center of mass velocity of the disk 1 before the impact (v_o) and the corresponding velocities of the disks just after the impact (v_1, v_2), by means of the following relationships:

$$P_n = m_2 v_{2n} = -(m_1 v_{1n} - m_1 v_{on}), \tag{1}$$

$$P_t = m_2 v_{2t} = -(m_1 v_{1t} - m_1 v_{ot}). \tag{2}$$

If the disks have inertia moments I_1 ($=m_1R_1/k_1$) and I_2 ($= m_2R_2/k_2$), the angular velocities before (ω_o) and after the impact, (ω_1,ω_2), will be related by

$$P_t = \frac{1}{k_2} m_2 R_2 \omega_2 = -\frac{1}{k_1} m_1 (R_1 \omega_1 - R_1 \omega_o). \tag{3}$$

In the IFR closure, it will be assumed that the net impulses P_t, P_n, result from the sum of independent contributions due to friction and restitution mechanisms. In the normal direction, only normal restitution operates, while in the tangential direction, linear impulses due to restitution, P_{te}, and friction, P_f, will be considered, as schematized in Fig. 2. The inelasticity of the impact can be described in terms of the normal coefficient of restitution, e_n, as $V_{2n} - V_{1n} = e_n V_{on}$, where the normal components of the disk's velocities of the contacting point before (V_{on}) and after the impact (V_{1n},V_{2n}) are introduced. For a central impact between homogeneous disks, such velocity components, equal the corresponding normal velocities of the mass centers so that, introducing the angles of impact (ψ) and scattering depicted in Fig. 1, the above definition leads to

$$v_2 \cos\delta_2 - v_1 \cos\delta_1 = e_n v_o \cos\psi. \tag{4}$$

Combining Eqs. (1) and (4) and introducing the mass ratio, M ($=m_1/m_2$), the normal impulse can be expressed as a function of the normal coefficient of restitution as

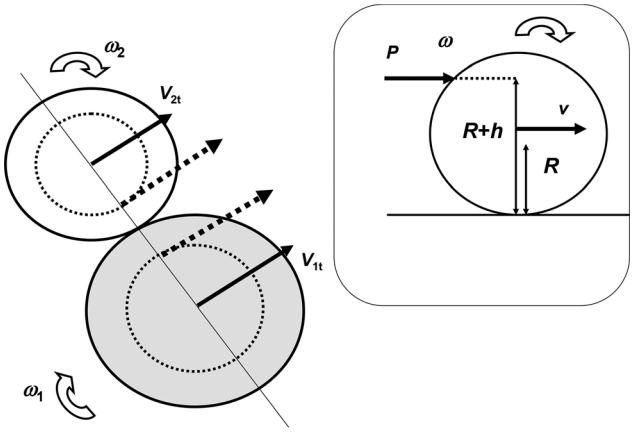

FIG. 2. Schemes to define the percussion center of a disk (up) and the condition of type-B sticking (down) in the oblique impact of two disks moving on a horizontal surface.

$$|P_n| = m_1 \left(\frac{1+e_n}{1+M}\right) v_o \cos\psi, \tag{5}$$

while the normal components of the center of mass velocity of the disks will be

$$v_{1n} = \left(\frac{M-e_n}{1+M}\right) v_o \cos\psi; \tag{6}$$

$$v_{2n} = M\left(\frac{1+e_n}{1+M}\right) v_o \cos\psi. \tag{7}$$

The impulse due to tangential restitution, P_{et}, will be expressed in terms of the coefficient of tangential restitution, e_t, defined here as the negative ratio of the postimpact to preimpact tangential components of the relative velocity of the contacting points of the disks *when friction effects are negligible*. Upon these idealized circumstances, e_t can be related to the tangential components of velocity of the contacting points, V_{ot}, V_{1t}, V_{2t}, by means of the relationship $V_{2t} - V_{1t} = e_t V_{ot}$. Since $V_j = v_j + R_j\omega_j$ (j = 0, 1, 2), combining the above definition with Eqs. (2) and (3) yields

$$|P_{et}| = m_1(1+e_t)\left(\frac{v_o \sin\psi + R_1\omega_o}{1+k_1+M(1+k_2)}\right). \tag{8}$$

B. Sliding regime

This expression corresponds to the linear impulse associated with the tangential restitution mechanism. As previously noted, it will be assumed that both the normal impulse given by Eq. (5) and the tangential restitution impulse provided by Eq. (8) act simultaneously during the impact regardless of the collision regime. The effective tangential impulse should incorporate, however, the contribution of the friction mechanism. The friction impulse, P_f, when sliding occurs will be taken, as usual, as

$$|P_f| = \mu m_1 \left(\frac{1+e_n}{1+M}\right) v_o \cos\psi. \tag{9}$$

Then, the net tangential impulse will be the sum of P_{et} and P_f. It has to be noted that the sign of these impulses will depend on the direction of V_{ot}. In the following, for simplicity, we consider the case in which $V_{ot} > 0$. Then, the center of mass tangential components of velocity after impact will be

$$v_{1t} = v_o \sin\psi - (1+e_t)\left(\frac{v_o \sin\psi + R_1\omega_o}{1+k_1+M(1+k_2)}\right) - \mu M\left(\frac{1+e_n}{1+M}\right) v_o \cos\psi; \tag{10}$$

$$v_{2t} = (1+e_t)M\left(\frac{v_o \sin\psi + R_1\omega_o}{1+k_1+M(1+k_2)}\right) + \mu M\left(\frac{1+e_n}{1+M}\right) v_o \cos\psi. \tag{11}$$

C. Sticking regime

The description of collisions in the stick regime is made difficult by the fact that we do not dispose of a constitutive equation equivalent to the Coulomb law for sliding friction.[36,53,56] Two different approximations can be taken. The first one is equivalent to that used in classic

Published under license by AIP Publishing

models[29,30] to describe collisions in stick regime and can be expressed as $v_{1t} - R_1\omega_1 = V_{2t} + R_2\omega_2$. In the IFR modeling, this condition is reformulated assuming that the postcollision components of tangential velocity of the contact points of the disks are equal in the absence of restitution effects.[57,58] This condition, in the following labeled as "contact point model," leads to

$$|P_f| = m_1\left(\frac{v_o \sin\psi + R_1\omega_o}{1 + k_1 + M(1 + k_2)}\right), \tag{12}$$

and the tangential components of the center of mass velocities will be

$$v_{1t} = v_o \sin\psi - (2 + e_t)\left(\frac{v_o \sin\psi + R_1\omega_o}{1 + k_1 + M(1 + k_2)}\right), \tag{13}$$

$$v_{2t} = (2 + e_t)\left(\frac{v_o \sin\psi + R_1\omega_o}{1 + k_1 + M(1 + k_2)}\right). \tag{14}$$

A second approximation is based on the well-known concept of percussion center in rigid body mechanics. In short, the percussion center is a point of the body where the application of an impulsive force results in the subsequent pure rolling motion of the body. In this percussion center approach, the condition of impact with sticking is formulated as assuming that the tangential velocities of the percussion centers in the absence of restitution effects are equal just after the impact.[59,60] This model will be termed in the following as "percussion center model." In the case of homogeneous disks, these are located at a distance R/k from the center (see scheme in Fig. 2) so that the friction impulse is given by

$$|P_f| = m_1\left(\frac{v_o \sin\psi + R_1\omega_o}{2(1 + M)}\right). \tag{15}$$

Then, the tangential components of the center of mass velocities will be

$$v_{1t} = v_o \sin\psi - \left(\frac{2(1 + e_t)(1 + M) + 1 + k_1 + M(1 + k_2)}{2(1 + M)[1 + k_1 + M(1 + k_2)]}\right) \times (v_o \sin\psi + R_1\omega_o), \tag{16}$$

$$v_{2t} = M\left(\frac{2(1 + e_t)(1 + M) + 1 + k_1 + M(1 + k_2)}{2(1 + M)[1 + k_1 + M(1 + k_2)]}\right) \times (v_o \sin\psi + R_1\omega_o). \tag{17}$$

D. Postimpact angles. Particular cases

The obtained equations are notably simplified for the case of homogeneous disks ($k_1 = k_2 = 2$) colliding without initial spin ($\omega_o = 0$), yielding simple expressions for the rebound angles which can be experimentally tested. The postcollision angles when the impact takes place in the sliding regime are

$$\tan\delta_1 = \frac{v_{1t}}{v_{1n}} = \left(\frac{3(1 + M) - (1 + e_t)}{3(M - e_n)}\right)\tan\psi - \mu\left(\frac{1 + e_n}{M - e_n}\right), \tag{18}$$

$$\tan\delta_2 = \frac{v_{2t}}{v_{2n}} = \mu + \frac{1}{3}\left(\frac{1 + e_t}{1 + e_n}\right)\tan\psi. \tag{19}$$

For the contact point model of sticking collisions,

$$\tan\delta_1 = \left[\frac{3(1 + M) - (2 + e_t)}{3(M - e_n)}\right]\tan\psi, \tag{20}$$

$$\tan\delta_2 = \frac{1}{3}\left(\frac{2 + e_t}{1 + e_n}\right)\tan\psi. \tag{21}$$

For the percussion point model of sticking collisions,

$$\tan\delta_1 = \frac{6(1 + M) - (5 + 2e_t)}{6(M - e_n)}\tan\psi, \tag{22}$$

$$\tan\delta_2 = \left(\frac{5 + 2e_t}{6(1 + e_n)}\right)\tan\psi. \tag{23}$$

All the precedent expressions can be extended to the case of the rebound of a disk on an infinitely massive plane simply taking $M = 0$.[59] It is pertinent to underline here that, in contrast with the abundant literature on the impact of rigid bodies on infinitely massive half-spaces, the current approach considers impacts between objects of finite masses where the mass ratio M plays a crucial role.

The transition between the sliding and sticking regimes is independent of the masses of the disks. In the case of the contact point and percussion point sticking, the transition occurs at impact angles $\psi_{transit}$ given by

$$\tan\psi_{transit} = 3\mu\left(\frac{1 + e_n}{1 + e_t}\right), \tag{24}$$

$$\tan\psi_{transit} = 2\mu(1 + e_n), \tag{25}$$

respectively.

E. The "anomalous" tangential restitution

It is pertinent to note that the IFR model reduces to the Walton's[38] and Brach's[29] models for sliding collisions taking $e_t = -1$ and reduces to the Brach's model of no sliding[29] taking $e_t = 0$. As previously noted, Walton's discontinuous model[38–40] as well as the continuous–discontinuous models based on the formulation of Maw *et al.*[10,11,28,33,34,42,43,46,47] involves tangential restitution coefficients. These are usually defined as the (often minus) ratio of the tangential component of the velocities of the contact point before and after impact, although often defined in terms of the center of mass velocities. This tangential coefficient of restitution, $e_t(^*)$ in the following, varies significantly with the impact angle.

As far as the coefficients of tangential restitution are defined in previous models in the literature based on the "net" tangential velocities of the contact points, the $e_t(^*)$ coefficient is representative of the net tangential impulse. As a result, $e_t(^*)$ not only depends on the materials constituting the colliding bodies but also on the impact angle. This is to some extent in contradiction with the conception of the normal coefficient of restitution (and the coefficient of sliding friction) in the same classic models, where these parameters only depend on the materials. The values of the $e_t(^*)$ coefficient may in principle range between 1 for a tangentially elastic impact and 0, corresponding to the totally inelastic impact in the tangential direction, but energy considerations including friction effects have to be considered, as discussed by Louge and Adams.[44] In the IFR closure, the different definitions of e_t (as the negative ratio of the tangential velocities of the contact points in the absence of friction effects) ensure that this coefficient is independent of the impact angle. Then, the value $e_t = -1$ value corresponding formally to the absence of tangential restitution effects but not of

Published under license by AIP Publishing

friction ones. Again, energy considerations have to be introduced, as discussed for the oblique impact of spheres on infinitely massive planes.[58]

This coefficient of restitution, $e_t(^*)$, can easily be correlated with the coefficient of restitution defined in the IFR closure (defined from the velocities in the absence of friction effects), e_t, from the tangential velocities of the contacting points of the disks. In the case of collisions with sliding, Eqs. (2), (3), (8), and (9) yield

$$e_t(^*) = e_t + 3\mu(1 + e_n)\text{cotan}\psi \tag{26}$$

This means that the variation of the coefficient of tangential restitution with the impact angle obtained when experimental data are analyzed with other models[10,11,28,33,34,42,43,46,47] is "apparent" and can be justified in the theoretical frame of the IFR closure. In fact, Eq. (26) predicts a linear variation of the "apparent" coefficient of tangential restitution, $e_t(^*)$, with cotanψ which is in agreement with experimental data reported in the literature (see Fig. 8 in Ref. 47, Fig. 3 in Ref. 34, Fig. 6 in Ref. 43, Fig. 8 in Ref. 11, Fig. 5 in Ref. 41, and Fig. 6 in Ref. 42). Figure 3 compares the $e_t(^*)$ values reported by Kharaz *et al.*[42] for the impact of 5-mm aluminum oxide spheres on a thick soda–lime glass anvil and Antonyuk *et al.*[46] for the impact of Al_2O_3 granules on a hardened steel plate. Data corresponding to the sliding regime display a linear variation with cotanγ that can be reproduced using Eq. (26) with $e_n = 0.98$, $e_t = -0.96$, $\mu = 0.09$, and $e_n = 0.77$, $e_t = -0.86$, $\mu = 0.16$, respectively. As previously noted, this variation of the "apparent" tangential coefficient of restitution with the impact angle can be justified in the IFR model based on a constant coefficient e_t.

For sticking collisions, the contact point and the percussion point friction models lead to

$$e_t(*) = 1 + e_t, \tag{27}$$

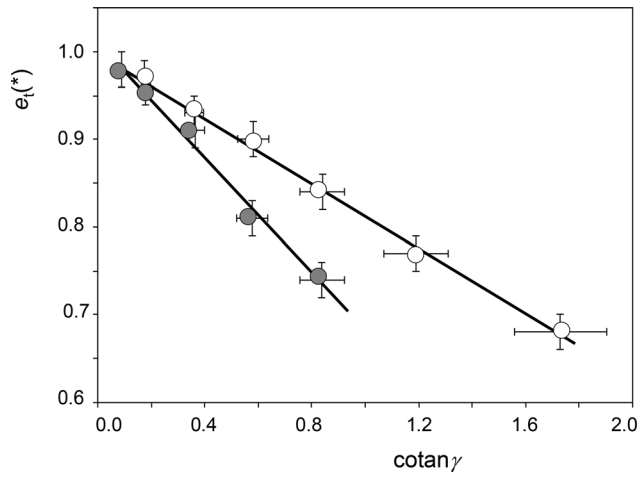

FIG. 3. Plots of $e_t(^*)$ vs cotanγ in the sliding regime region using experimental data reported by Kharaz *et al.*[42] for the impact of 5-mm aluminum oxide spheres on a thick soda–lime glass anvil (circles) and Antonyuk *et al.*[46] for the impact of Al_2O_3 granules on a hardened steel plate (solid circles). Theoretical lines from Eq. (26) inserting $e_n = 0.98$, $e_t = -0.96$, $\mu = 0.09$, and $e_n = 0.77$, $e_t = -0.86$, $\mu = 0.16$, respectively. Error bars were assumed to be of a 10% in cotanγ and ± 0.02 units in $e_t(^*)$.

$$e_t(*) = \frac{3}{2} + e_t, \tag{28}$$

respectively. It is pertinent to note that the stick occurs when the surface properties (roughness, porosity, asperities[48]) determine the appearance of sufficiently high friction effects to inhibit the slippage between the surfaces in contact. As underlined by Schwager *et al.*,[53] the no disposal of a constitutive model for friction in these conditions (equivalent to Coulomb's law for sliding friction) opens the possibility to use different definition criteria. The two alternative models used to describe impact in sticking regime (contact point and percussion point models) only differ by a numerical coefficient (1, 3/2) representative of the different adopted friction impulse model.

F. Stopping distances

After the impact, the disks slip over the horizontal surface with a combination of translation and rotation so that the center of mass of each disk continues in rectilinear motion, until both movements come to a simultaneous stop.[65] Under sliding friction conditions between the disks and the supporting horizontal plane, the disks undergo uniform linear and angular decelerations so that translation and rotation come to a simultaneous stop after covering distances d_1, d_2 which can be easily measured. These distances must verify the relationship[64]

$$\frac{v_2}{v_1} = \left(\frac{d_2}{d_1}\right)^{1/2}, \tag{29}$$

so that the experimental values of the $(d_2/d_1)^{1/2}$ ratio can be compared with the theoretical v_2/v_1 ratios calculated from Eqs. (6), (7), (10), (11), and (13), (14) or (16), (17).

As previously described,[64] this two-disk arrangement can be operationally viewed as an "inertial balance" devoted to determine inertial mass (as different to conventional balances measuring gravitational masses) based on collisions of the object body with the reference body of mass unit so that the mass ratio can be determined from angle, velocity, and/or stopping distance measurements

$$\frac{m_2}{m_1} = \left(\frac{v_2 \sin\alpha_2}{v_1 \sin\alpha_1}\right) = \left(\frac{d_2}{d_1}\right)^{1/2}\left(\frac{\sin\alpha_2}{\sin\alpha_1}\right). \tag{30}$$

G. Rolling friction effects

The center of mass motion previously considered is unaffected by rolling friction effects. These can be introduced, as previously described,[61] by considering two regimes: rolling and nonrolling. In the first case, rolling friction effects are described in terms of an additional friction torque given by

$$T_f = \rho P_n, \tag{31}$$

where ρ is the coefficient of rolling friction. It is assumed that this is a material's constant, independent of the incoming velocity, impact angle, mass, and radii of the disks, having dimensions of length. For simplicity, it will be considered only the case in which two homogeneous disks collide without initial spin. In this case, the nonrolling regime is described in terms of a friction torque that can be expressed as

Published under license by AIP Publishing

$$|T_f| = m_1 r\left(\frac{v_o \sin\psi + R_1\omega_o}{3(1+M)}\right), \quad (32)$$

where $r = 2R_1R_2/(R_1 + R_2)$. Notice that the sign of these angular impulses will depend on the direction of the tangential component of the velocity of the contacting point, V_{ot}. The case of $R_1 = R_2 = R$, then $r = R$.

The introduction of rolling friction effects leads to four cases: sliding plus rolling, sliding plus nonrolling, sticking plus rolling, and sticking plus nonrolling. For brevity, only the expressions for the post-collision angular velocity of the disk 2, the more easily measured quantity, will be provided. In the case of sliding, the net tangential impulse, P_t, becomes

$$|P_t| = m_1\left(\frac{1+e_t}{3(1+M)}\right)v_o\sin\psi - m_1\mu M\left(\frac{1+e_n}{1+M}\right)v_o\cos\psi. \quad (33)$$

Then, for the case of sliding plus rolling impact, combination of Eqs. (31) and (33) gives

$$R_2\omega_2 = \frac{2}{3}M\left(\frac{1+e_t}{1+M}\right)v_o\sin\psi + 2\left(\mu - \frac{\rho}{R_2}\right)M\left(\frac{1+e_n}{1+M}\right)v_o\cos\psi. \quad (34)$$

In turn, the case of sliding plus nonrolling can be derived from Eqs. (32) and (33),

$$R_2\omega_2 = \frac{2}{3}M\left(\frac{1+e_t-(r/R_2)M}{1+M}\right)v_o\sin\psi + 2\mu M\left(\frac{1+e_n}{1+M}\right)v_o\cos\psi. \quad (35)$$

In the contact point model of sticking, the net tangential impulse is

$$|P_t| = m_1\left(\frac{v_o\sin\psi}{3(1+M)}\right)(2+e_t), \quad (36)$$

so that the sticking plus rolling and sticking plus nonrolling regimes are described, respectively, by

$$R_2\omega_2 = \frac{2}{3}M\left(\frac{2+e_t}{1+M}\right)v_o\sin\psi - 2\frac{\rho}{R_2}M\left(\frac{1+e_n}{1+M}\right)v_o\cos\psi, \quad (37)$$

$$R_2\omega_2 = \frac{2}{3}M\left(\frac{2+e_t-(r/R_2)M}{1+M}\right)v_o\sin\psi. \quad (38)$$

Finally, the percussion point model of sticking is represented by means of a net tangential impulse

$$|P_t| = m_1\left(\frac{v_o\sin\psi}{6(1+M)}\right)(5+2e_t). \quad (39)$$

Accordingly, the percussion point sticking plus rolling and percussion point sticking plus nonrolling regimes are described by the equations

$$R_2\omega_2 = \frac{1}{3}M\left(\frac{5+2e_t}{1+M}\right)v_o\sin\psi - 2\frac{\rho}{R_2}M\left(\frac{1+e_n}{1+M}\right)v_o\cos\psi, \quad (40)$$

$$R_2\omega_2 = \frac{2}{3}M\left(\frac{5+2e_t-(r/R_2)M}{1+M}\right)v_o\sin\psi, \quad (41)$$

respectively.

Similar sets of equations can be developed for the apparent values of the coefficient of tangential restitution. The corresponding expressions for the different impact regimes are summarized in Table I.

III. EXPERIMENTAL DETAILS

The oblique impact between different coins was studied. Their masses were determined with a balance being coincident with the nominal masses at the level of ±0.01 g. Bronze–aluminum (5 pts, Spain 1981, mass 3.00 ± 0.01 g, diameter 17.50 mm; 100 pts, Spain 1983; mass 9.23 ± 0.01 g, diameter 24.50 mm; 500 pts, Spain 1985, mass 12.00 ± 0.01 g, diameter 28.00 mm), copper-nickel (50 cts, Spain 1975; mass 7.80 ± 0.01 g; diameter 24.25 mm; 200 pts, Spain 1980, mass 10.50 ± 0.01 g, diameter 25.50 mm,), and aluminum (mass 1.19 ± 0.01 g, diameter 21.00 mm) were used. Additional experiments were performed with polyester resin disks (mass 4.03 ± 0.02 g, diameter 30.00 mm). The angles of impact and rebound were measured from images taken with an Olympus OM-D E-M1 Mark III digital camera (CSC 80 MPixels) placed in zenithal position at a height of 75 cm over the laboratory bench. The images were taken at exposure times of 0.5 and 1.0 s. The disks were projected with velocities between 0.20 and 1.5 m s^{-1} without initial spin using a rubber band powdered launcher. The number of data points, N, ranged between 15 and 25, being indicated in the respective figure captions. Uncertainties in angle measurements in replicate experiments ranged typically between 0.5° and 1°.

IV. RESULTS AND DISCUSSION

First, we studied the possible variation of the experimental parameters with the impact velocity v_o. Figure 4 shows the values of the angle α measured for different impact velocities in the collisions between two bronze–aluminum coins ($M = 1.00$) at impact angles of 16°, 30°, 45°, and 60°, all assumed to be ±1°. The average values from three replicate measurements carried out at each velocity are represented, the error bars corresponding to the separation between the

TABLE I. Theoretical expressions of the apparent coefficient of tangential restitution, $e_t(^*)$, for the different impact regimes in the collisions between two homogeneous disks. Notice that the equations in the first column reduce to Eqs. (26)–(28) taking $\rho = 0$.

Regime	$e_t(^*)$	Regime	$e_t(^*)$
Skiding plus rolling	$e_t + \left(3\mu - 2\frac{\rho}{r}\right)(1+e_n)\cot\psi$	Sliding plus nonrolling	$e_t - 2 + 3\mu(1+e_n)\cot\psi$
Sticking plus rolling, contact point model	$1 + e_t - 2\frac{\rho}{r}(1+e_n)\cot\psi$	Sticking plus nonrolling, contact point model	$e_t - 1$
Sticking plus rolling, percussion point model	$\frac{3}{2} + e_t - 2\frac{\rho}{r}(1+e_n)\cot\psi$	Sticking plus nonrolling, percussion point model	$e_t - \frac{1}{2}$

Published under license by AIP Publishing

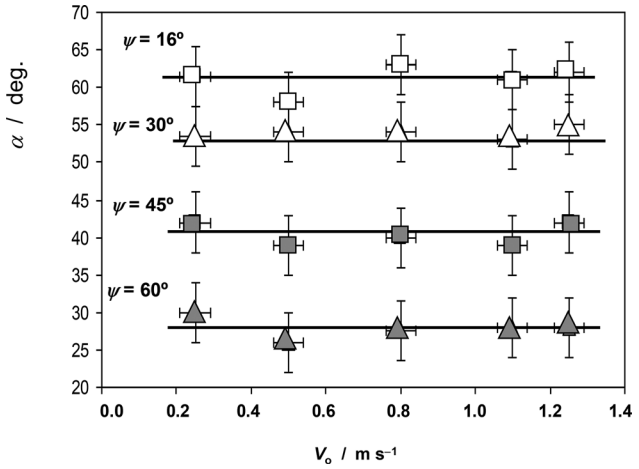

FIG. 4. Values of the angle α measured at five different impact velocities (v_o) measured in the impact between two bronze–aluminum coins ($M = 1.00$) at impact angles of 16°, 30°, 45°, and 60°.

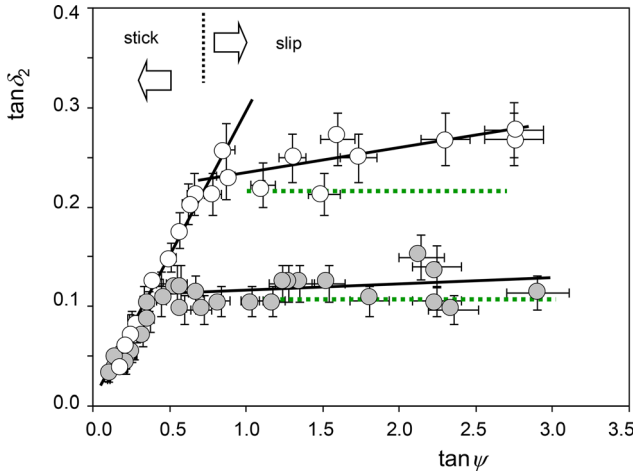

FIG. 5. Plots of $\tan\delta_2$ vs $\tan\psi$ for impacts between two equal (a) copper–aluminum and (b) aluminum coins. Experimental data points ($N = 25$) and theoretical values from Eqs. (19) (sliding regime) and (23) (stick regime) inserting $e_n = 0.80$, $e_t = -0.98$, and $\mu = 0.11$ (copper–aluminum) and $e_n = 0.87$, $e_t = -0.88$, and $\mu = 0.21$ (aluminum). The sliding region shows the "anomalous" deviation relative to the standard models whose prediction is denoted by dotted lines.

extreme values. These data clearly suggest that, at each impact angle, there is no variation of the α values with the impact velocity. As, ultimately, the postimpact angle values will depend on the coefficients of restitution and friction, the above experimental result suggests that such coefficients can be taken as essentially velocity-independent under our experimental conditions. Such data are coincident with much experimental results reported in the literature where the normal coefficient of restitution was found to be independent of the incoming velocity.[11,31,33–35,39–43,46,47] The following experimental data correspond to measurements at $v_o = 1.0 \pm 0.1$ m s^{-1}.

Figure 5 depicts the variation of $\tan\delta_2$ on $\tan\psi$ for oblique impacts between two equal (a) copper–aluminum and (b) aluminum coins. Consistently with the previous theoretical treatment, experimental data at low and large impact angles can be fitted to two different straight lines corresponding, respectively, to the collisions in sticking and sliding regimes. To compare the alternative contact point model [Eq. (21)] and the percussion point model [Eq. (23)] describing the sticking regime, the parameters of the fitted straight lines (slope, ordinate at the origin) corresponding to the sliding and sticking regions were combined to calculate a set of e_n, e_t, and μ values. In all cases, the values for these parameters calculated from Eqs. (19) and (23) were consistent with those calculated from the linear variations of $\tan\delta_1$ on $\tan\psi$ [Eqs. (18) and (22)]. In contrast, the e_n, e_t, and μ values calculated for the contact point model from Eqs. (19) and (21) and from Eqs. (18) and (20) exhibited some discrepancies. Accordingly, the percussion center model was selected as more appropriate to describe experimental data under our experimental conditions.

As illustrated in Fig. 5, experimental data can be satisfactorily correlated with theoretical predictions from Eqs. (19) (sliding regime) and (23) (percussion point-type stick regime) inserting $e_n = 0.80$, $e_t = -0.98$, and $\mu = 0.11$ for copper–aluminum coins and $e_n = 0.87$, $e_t = -0.88$, and $\mu = 0.21$ for aluminum coins. These values fall within the range of values of these coefficients calculated for different pairs of materials applying the IFR model to the literature data.[57–60] These values are coincident with the respective values of e_n and μ calculated in the literature applying classic models[11,31,33–35,39–43,46,47] where the values of μ ranged between 0.05[40] and 0.20,[39] while the values of e_n ranged between 0.53[46] and 0.97[33,40] (see Ref. 59 for a comparative table).

Experimental data at low impact angles can also be fitted to Eq. (21), corresponding to the contact point model of the sticking regime, but the values of e_n and e_t offered relatively large variations between the different sets of coins, so that the percussion point model of sticking was used. Table II summarizes the characteristics of the studied disks and the estimated values of the coefficients of friction, and normal restitution, and tangential restitution.

Figure 5 illustrates how the IFR model agrees with experimental data in the sliding region (large impact angles) where the plots of $\tan\delta_2$ on $\tan\psi$ fit to an inclined straight line. This representation is equivalent to the variation of the tangential to normal impulse ratio on $\tan\psi$ that, in classic models, is predicted to be constant and equal to μ (prediction denoted by dotted lines). The data in Fig. 5 are coincident with those in the literature data that were considered as "anomalous"[35,39,40,44,45] in the standard models where restitution and friction are coupled. In contrast, the IFR closure, on separating the contributions of restitution and friction, permits to include these results within the "ordinary" impact behavior.

In accordance with the theoretical model, the values of δ_2 recorded for impacts of coins of the same material but different masses were found to be independent of the mass ratio M. In contrast, and also in agreement with theory, the values of the angle δ_1 varied with the mass ratio, as can be seen in Fig. 6. Experimental data points can be satisfactorily correlated with theoretical curves from Eqs. (18) (sliding regime) and (22) (stick regime) inserting $e_n = 0.90$, $e_t = -0.90$, and $\mu = 0.15$. The agreement between theory and experimental data in the sticking region is illustrated in Fig. 7, where the plots of $\tan\delta_1$ vs $\tan\psi$ for the impacts of the above bronze–aluminum coins are shown. Here, error bars correspond to the averaged separation between the

Published under license by AIP Publishing

TABLE II. Main characteristics of the studied disks, optimized values of the coefficients of restitution and friction and the sticking-sliding transition angle.

Disks	Material	M	e_n	e_t	μ	$\psi_{transit}$ (deg)
25 cts–25 cts coins	Copper–nickel	1.00	0.86	−0.99	0.19	35.2
1 pta–1 pta coins	Aluminum	1.00	0.87	−0.88	0.21	38.1
5 pts–5 pts coins	Bronze–aluminum	1.00	0.80	−0.98	0.11	21.6
200 pts–200 pts coins	Copper–nickel	1.00	0.77	−0.96	0.15	28.0
500 pts-100 pts coins	Bronze–aluminum	1.28	0.90	−0.90	0.15	29.6
100 pts-100 pts coins	Bronze–aluminum	1.00	0.90	−0.90	0.15	29.6
100 pts-500 pts coins	Bronze–aluminum	0.79	0.90	−0.90	0.15	29.6
Polyester resin disks	Polyester resin	1.00	0.67	−0.95	0.14	25.1

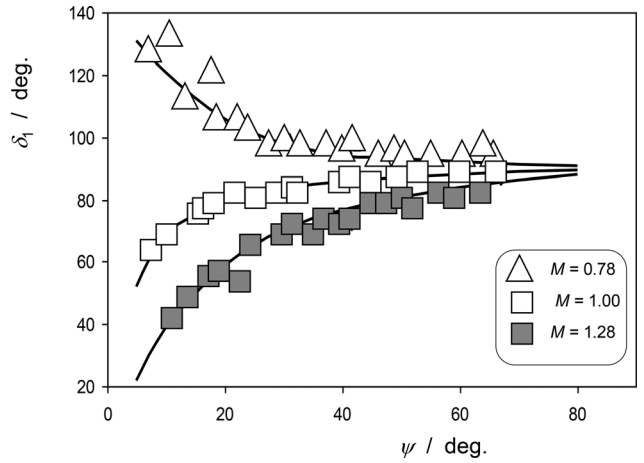

FIG. 6. Plots of δ_1 vs ψ for impacts between bronze–aluminum coins of different mass ratios. Experimental data points ($N = 20$) and theoretical values (continuous lines) from Eqs. (18) (sliding regime) and (22) (stick regime) inserting $e_n = 0.90$, $e_t = -0.90$, and $\mu = 0.15$.

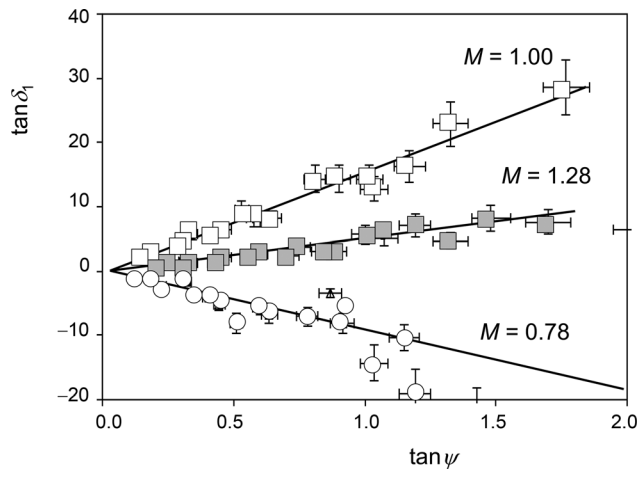

FIG. 7. Plots of $\tan\delta_1$ vs $\tan\psi$ for impacts between bronze–aluminum coins of different mass ratios in the region of sticking regime (low impact angles). Experimental data points ($N = 18$) and theoretical values (continuous lines) from Eq. (22) inserting $e_n = 0.90$ and $e_t = -0.90$.

extreme values in three replicate measurements. In Fig. 6, as well as in Figs. 8 and 9, the error bars fall within the represented figures.

The angle α_1 is particularly sensitive to the differences between the materials. This can be seen in Fig. 8 where the variation of this angle with the impact angle for oblique collisions of aluminum coins and polyester resin disks (in both cases with $M = 1.00$) is shown. Experimental data can be fitted satisfactorily to theoretical curves for collisions in sliding [Eq. (18)] and sticking regime [Eq. (22)] taking $e_n = 0.87$, $e_t = -0.88$, and $\mu = 0.21$ (aluminum) and $e_n = 0.67$, $e_t = -0.95$, and $\mu = 0.14$ (polyester resin). These differences can be associated with the different elastoplastic properties, ultimately Young's modulus and Poisson's coefficient, between the "bulk" materials, and the roughness/asperity of the surfaces. According to the IFR closure, the former properties will determine the values of the normal and tangential coefficients of restitution while the latter will determine the values of the friction coefficient.

Similarly, the angle α_1 is also sensitive to changes in the mass ratio. This can be seen in Fig. 9 in which the α_1 vs ψ plots for oblique collisions of bronze–aluminum coins with $M = 1.28$, $M = 1.00$, and

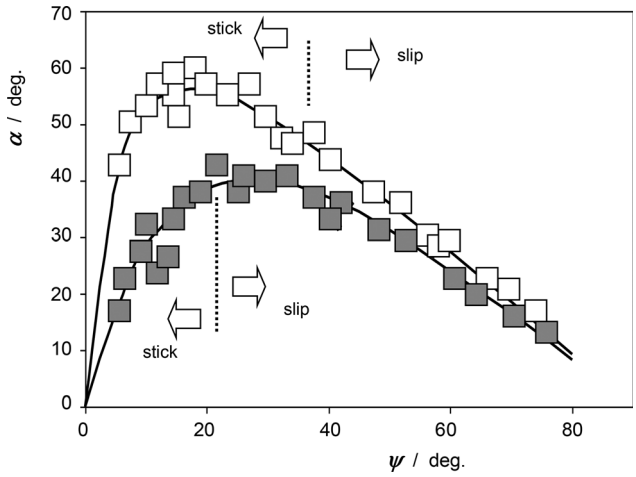

FIG. 8. Variation of the angle α_1 with the impact angle for oblique collisions of aluminum coins (squares, $M = 1.00$) and polyester resin disks (solid squares, $M = 1.00$). Experimental data points ($N = 25$) and theoretical lines for collisions in sliding [Eq. (18)] and sticking regime [Eq. (22)] taking $e_n = 0.87$, $e_t = -0.88$, and $\mu = 0.21$ (aluminum) and $e_n = 0.67$, $e_t = -0.95$, and $\mu = 0.14$ (polyester resin).

Published under license by AIP Publishing

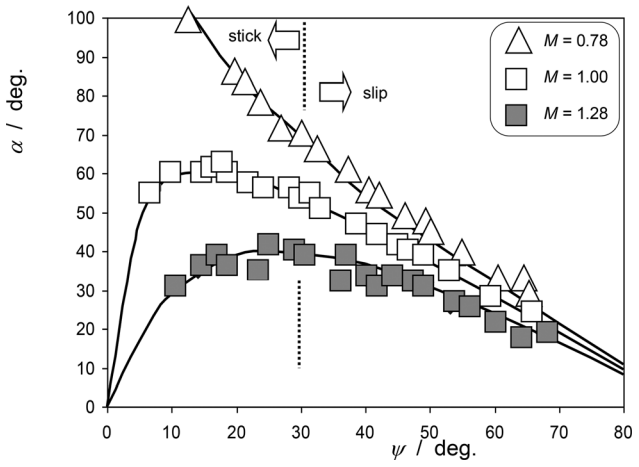

FIG. 9. Variation of the angle α_1 with the impact angle for oblique collisions of bronze–aluminum coins with $M = 1.28$, $M = 1.00$, and $M = 0.78$. Experimental data points ($N = 20$) and theoretical lines for collisions in sliding [Eq. (18)] and sticking regime [Eq. (22)] taking $e_n = 0.90$, $e_t = -0.90$, and $\mu = 0.15$.

$M = 0.78$ are compared. For all three mass ratios, experimental data are consistent with theoretical curves from Eq. (18) (sliding regime) and Eq. (22) (sticking regime) taking a unique set of values of the coefficients of restitution and friction: $e_n = 0.90$, $e_t = -0.90$, and $\mu = 0.15$.

Similar agreement between theory and experiment was obtained using the variation of the $(d_2/d_1)^{1/2}$ ratio on the impact angle. This is exemplified by the data for aluminum coins ($M = 1$) shown in Fig. 10. Here, experimental data are superimposed with the theoretical prediction combining Eqs. (6), (7), (10), (11) (sliding) and (6), (7), (16), (17) (sticking) taking inserting $e_n = 0.87$, $e_t = -0.88$, and $\mu = 0.21$. These results underline the importance of the mass ratio to modulate the postimpact velocities both in direction (postimpact angles) and absolute value. As previously noted, this system can also be seen as an inertial balance to measure inertial masses.

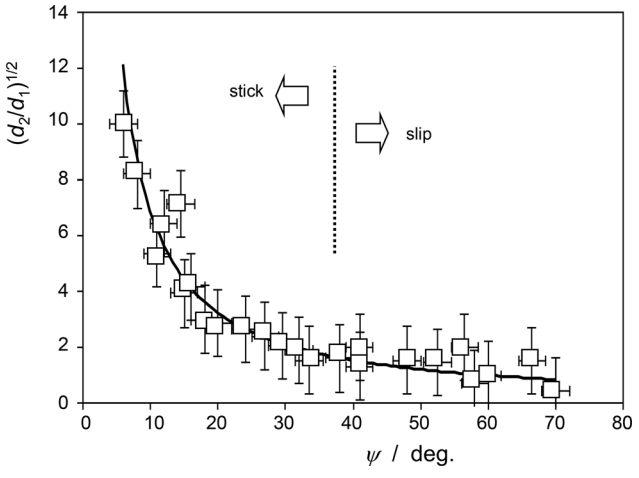

FIG. 10. Variation of the $(d_2/d_1)^{1/2}$ ratio with the angle of impact for collisions between aluminum coins of $M = 1$. Experimental data ($N = 25$) and theoretical line inserting $e_n = 0.87$, $e_t = -0.88$, and $\mu = 0.21$ into Eqs. (6), (7), (10), (11) (sliding) and (6), (7), (16), (17) (sticking).

Rolling friction effects were studied from the experimental values of the $R_2\omega_2/v_o$ ratio. Figure 11 depicts the variation of this ratio with the impact angle determined for collisions between two bronze–aluminum coins with $M = 1.00$. Experimental data are consistent with theoretical lines for collisions in sliding plus rolling [Eq. (34)] and sticking plus rolling [Eq. (40)] regimes taking $e_n = 0.90$, $e_t = -0.90$, $\mu = 0.15$, and $\rho/R_2 = 0.02$. The stick plus nonrolling regime, which should occur at very small impact angles,[61] cannot be detected here. Under our experimental conditions, however, rolling friction effects cannot be accurately detected, experimental data being close to the theoretical predictions neglecting such effects (dotted lines in Fig. 11). In all cases, the values of the ρ/R_2 ratio estimated from experimental data were in the 0.01–0.03 range.

Finally, the proposed IFR model describes satisfactorily the variation of the "apparent" coefficient of tangential restitution defined in the standard models, $e_t(^*)$, with the impact angle. For simplicity, and taking into account the previous results on $R_2\omega_2/v_o$, rolling friction effects will be neglected here. Figure 12 compares the experimental data from velocity measurements at the contact points of two colliding polyester resin disks of equal mass with theory from Eqs. (26) (sliding) and (28) taking $e_n = 0.67$, $e_t = -0.95$, and $\mu = 0.14$. In the sliding region, a linear variation of $e_t(^*)$ on cotanψ is obtained. This representation is equivalent to those reported in the literature (see Fig. 8 in Ref. 47, Fig. 3 in Ref. 35, Fig. 6 in Ref. 43, Fig. 8 in Ref. 11, Fig. 5 in Ref. 41, and Fig. 6 in Ref. 42) and illustrates the suitability of the IFR closure to justify this "anomaly" which becomes within the "ordinary" behavior predicted by this model.

In spite of its simplicity, the IFR model permits to describe two-disk impact events with satisfactory fit to experimental data under conditions of low velocity and absence of adhesive effects. Two aspects can be underlined: (i) the model does not use any adjustable parameter and does not require the previous knowledge of some empirical

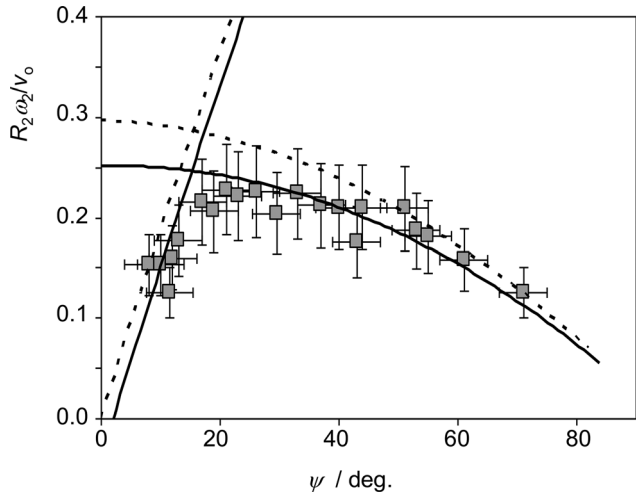

FIG. 11. Experimental data ($N = 21$) of the $R_2\omega_2/v_o$ ratio vs the impact angle determined for collisions between two bronze–aluminum coins with $M = 1.00$ and theoretical lines for collisions in sliding plus rolling [Eq. (34)] and sticking plus rolling [Eq. (40)] regimes taking $e_n = 0.90$, $e_t = -0.90$, $\mu = 0.15$, and $\rho/R_2 = 0.02$. The dotted lines correspond to the same theoretical predictions taking $\rho/R_2 = 0.02$, i.e., ignoring rolling friction effects.

Published under license by AIP Publishing

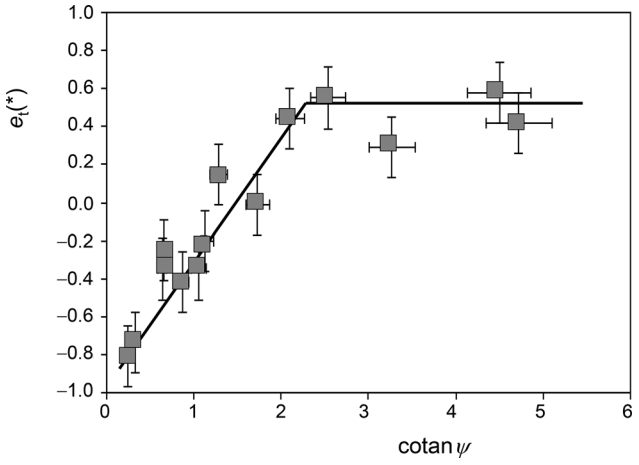

FIG. 12. Variation of the "apparent" coefficient of tangential restitution, $e_t(^*)$, with the impact angle for the oblique impact between polyester resin disks ($M = 1.00$). Experimental data points ($N = 15$) and the continuous lines correspond to the theoretical prediction from Eqs. (26) (sliding) and (28) (sticking) taking $e_n = 0.67$, $e_t = -0.95$, and $\mu = 0.14$.

information (Young's modulus and Poisson's coefficient) from experiments independent of the impact event, problems of the standard models:[10,54,55] (ii) the interpretation of several experimental data considered as "anomalous" within the context of the standard models,[35,39,40,44,45] now falling within the "ordinary" impact behavior.

V. CONCLUSIONS

The oblique collisions between axisymmetric disks can be modeled upon assuming that restitution and friction effects can be represented by tangential linear impulses acting independently. Introducing a restricted definition of the tangential coefficient of restitution in terms of the relative tangential components of the velocities of the contacting points of the disks in the absence of *friction* is possible to propose constitutive definitions for the impulse due to tangential restitution. Combining such impulses with those due to normal restitution and friction, the postimpact linear and angular velocities and scattering angles can be obtained as a function of the impact angle, masses, initial linear and angular velocity, and the coefficients of normal restitution, tangential restitution, and friction.

Experimental data for two-disk collisions of different materials and mass ratios are in satisfactory agreement with theoretical predictions from the sliding and sticking regimes using a unique set of velocity-independent coefficients of friction and normal and tangential restitution. The values of such coefficients can be seen within the IFR closure as resulting from the roughness/asperity of the surfaces in contact and the elastic properties of the bulk materials, respectively. The formulation proposed here permits to justify a series of experimental results considered as "anomalous" when studied using the standard models, that are regarded as being within the "ordinary" impact behavior predicted by the independent friction-restitution model.

ACKNOWLEDGMENTS

Financial support was received from the MINECO Project CTQ2017–85317-C2–1-P which is supported with *Ministerio de Economía, Industria y Competitividad* (MINECO) and *Fondo Europeo de Desarrollo Regional* (ERDF).

DATA AVAILABILITY

The data that support the findings of this study are available from the corresponding author upon reasonable request.

REFERENCES

[1]D. Vescovi, D. Berzi, P. Richard, and N. Brodu, "Plane shear flows of frictionless spheres: Kinetic theory and 3D soft-sphere discrete element method simulations," Phys. Fluids **26**, 053305 (2014).
[2]J. Koplika, "Surface impacts and collisions of particle-laden nanodrops," Phys. Fluids **27**, 082001 (2015).
[3]G. Charalampous and Y. Hardalupas, "Collisions of droplets on spherical particles," Phys. Fluids **29**, 103305 (2017).
[4]Z. Zhang and P. Zhang, "Kinetic energy recovery and interface hysteresis of bouncing droplets after inelastic head-on collision," Phys. Fluids **29**, 103306 (2017).
[5]S. Yang, L. Zhang, K. Luo, and J. W. Chew, "DEM study of the size-induced segregation dynamics of a ternary-size granular mixture in the rolling-regime rotating drum," Phys. Fluids **29**, 123301 (2017).
[6]X. Chen and V. Yang, "Direct numerical simulation of multiscale flow physics of binary droplet collision," Phys. Fluids **32**, 062103 (2020).
[7]B. C. Abrahamsen, H. S. Alsos, V. Aune, E. Fagerholt, O. M. Faltinsen, and O. Hellan, "Hydroplastic response of a square plate due to impact on calm water," Phys. Fluids **32**, 082103 (2020).
[8]C. S. Bester, N. Cox, H. Zheng, and R. P. Behringer, "Dynamics of oblique impact in a quasi two-dimensional granular medium," Granular Matter **22**, 51 (2020).
[9]C. Wang, A. Deng, A. Taheri, H. Zhao, and J. Li, "Modelling particle kinetic behaviour considering asperity contact: Formulation and DEM simulations," Granular Matter **21**, 27 (2019).
[10]O. V. Kim and P. F. Dunn, "A microsphere-surface impact model for implementation in computational fluid dynamics," J. Aerosol Sci. **38**, 532 (2007).
[11]J. Xie, M. Dong, S. Li, Y. Mei, and Y. Shang, "An experimental study of fly ash particle oblique impact with stainless surfaces," J. Aerosol Sci. **123**, 27 (2018).
[12]S. Chen and V. Bertola, "Drop impact on spherical soft surfaces," Phys. Fluids **29**, 082106 (2017).
[13]K. Wang, H. Chen, H. Ge, X. Liu, H. Liu, and S. Dhen, "Study of impact velocity and curvature ratio on the dynamic characteristics of double droplets impacting super-hydrophobic tubes," Phys. Fluids **33**, 013301 (2021).
[14]S. A. Banitabaei and A. Amirfazli, "Droplet impact onto a solid sphere: Effect of wettability and impact velocity," Phys. Fluids **29**, 062111 (2017).
[15]N. Chen, H. Chen, and A. Amirfazli, "Drop impact onto a thin film: Miscibility effect," Phys. Fluids **29**, 092106 (2017).
[16]A. V. Bazilevsky and A. N. Rohzkov, "Impact of a small disk on a sessile water drop," Phys. Fluids **32**, 087101 (2020).
[17]K. Egawa and H. Katsuragi, "Bouncing of a projectile impacting a dense potato-starch suspension layer," Phys. Fluids **31**, 053304 (2019).
[18]H.-C. Hsu and H. Capart, "Enhanced upswing in immersed collisions of tethered spheres," Phys. Fluids **19**, 101701 (2007).
[19]P. Zhang and C. K. Lawa, "An analysis of head-on droplet collision with large deformation in gaseous medium," Phys. Fluids **23**, 042102 (2011).
[20]A. M. Moqaddam, S. S. Chikatamarla, and I. V. Karlinc, "Simulation of binary droplet collisions with the entropic lattice Boltzmann method," Phys. Fluids **28**, 022106 (2016).
[21]H. Liu and Z. Lv, "Vibration and instability analysis of flow-conveying carbon nanotubes in the presence of material uncertainties," Phys. A **511**, 85 (2018).
[22]S. Oveissi and A. Ghassemi, "Longitudinal and transverse wave propagation analysis of stationary and axially moving carbon nanotubes conveying nanofluid," Appl. Math. Modell. **60**, 460 (2018).
[23]U. Torres-Herrera and E. Corvera Poire, "An analytical framework to determine flow velocity within nanotubes from their vibration frequencies," Phys. Fluids **30**, 122001 (2018).
[24]L. J. Yiew, L. G. Bennetts, M. H. Meylan, G. A. Thomas, and B. J. French, "Wave-induced collisions of thin floating disks," Phys. Fluids **29**, 127102 (2017).

Published under license by AIP Publishing

[25]S. Sur, H. Masoud, and J. P. Rothstein, "Translational and rotational motion of disk-shaped Marangoni surfers," Phys. Fluids **31**, 102101 (2019).
[26]W. Stronge, *Impact Mechanics* (Cambridge University Press, New York, 2000).
[27]R. M. Brach, *Mechanical Impact Dynamics* (John Wiley, New York, 2007).
[28]N. Maw, J. R. Barber, and J. N. Fawcett, "The rebound of elastic bodies in oblique impact," Mech. Res. Commun. **4**, 17 (1977).
[29]R. M. Brach, "Friction, restitution, and energy loss in planar collisions," J. Appl. Mech. **51**, 164 (1984).
[30]T. R. Kane and D. A. Levinson, "An explicit solution of the general two-body collision problem," Comput. Mech. **2**, 75 (1987).
[31]A. Le Quiniou, F. Rioual, P. Héritier, and Y. Lapusta, "Experimental study of the bouncing trajectory of a particle along a rotating wall," Phys. Fluids **21**, 123302 (2009).
[32]W. J. Stronge, R. James, and B. Ravani, "Oblique impact with friction and tangential compliance," Philos. Trans. R. Soc., A **359**, 1 (2001).
[33]G. G. Joseph and M. L. Hunt, "Oblique particle-wall collisions in a liquid," J. Fluid Mech. **510**, 71 (2004).
[34]C. Y. Wu, C. Thornton, and L.-Y. Li, "A semi-analytical model for oblique impact of elastoplastic spheres," Proc. R. Soc., A **465**, 937 (2009).
[35]J. Calsamiglia, S. W. Kennedy, A. Chatterjee, A. L. Ruina, and J. T. Jenlins, "Anomalous Frictional Behavior in Collisions of Thin Disks," J. Appl. Mech. **66**, 146 (1999).
[36]S. Luding, "Cohesive, frictional powders: Contact models for tension," Granular Matter **10**, 235 (2008).
[37]J. A. Simeonov, "The coefficient of normal restitution for Hertzian contact of two rough spheres colliding in a viscous fluid," Mech. Res. Commun. **73**, 140 (2016).
[38]O. R. Walton, "Numerical simulation of inelastic, frictional particle-particle interactions," in *Particulate Two-Phase Flow*, edited by M. C. Rocco (Butterwort-Heinemann, Stonehem, 1993), pp. 884–911.
[39]S. F. Foerster, M. Y. Louge, H. Chang, and K. Allia, "Measurements of the collision properties of small spheres," Phys. Fluids **6**, 1108 (1994).
[40]A. Lorenz, C. Tuozzolo, and M. Y. Louge, "Measurement of impact properties of small, nearly spherical particles," Exp. Mech. **37**, 292 (1997).
[41]D. A. Gorham and A. H. Kharaz, "The measurement of particle rebound characteristics," Powder Technol. **112**, 193 (2000).
[42]A. H. Kharaz, D. A. Gorham, and A. D. Salman, "An experimental study of the elastic rebound of spheres," Powder Technol. **120**, 281 (2001).
[43]H. Dong and M. H. Moys, "Experimental study of oblique impacts with initial spin," Powder Technol. **161**, 22 (2006).
[44]M. Y. Louge and M. E. Adams, "Anomalous behavior of normal kinematic restitution in the oblique impacts of a hard sphere on an elasto-plastic plate," Phys. Rev. E **65**, 021303 (2002).
[45]R. Mourya and A. Chatterjee, "Anomalous frictional behavior in collisions of thin disks revisited," J. Appl. Mech. **75**, 024501 (2008).
[46]S. Antonyuk, S. Heinrich, J. Tomas, N. G. Deen, M. S. van Buijtenen, and J. A. M. Kuipers, "Energy absorption during compression and impact of dry elastic-plastic spherical granules," Granular Matter **12**, 15 (2010).
[47]P. Mueller, S. Antonyuk, M. Stasiak, J. Tomas, and S. Heinrich, "The normal and oblique impact of three types of wet granules," Granular Matter **13**, 455 (2011).
[48]N. V. Brilliantov, V. Spahn, J.-M. Hertzsch, and T. Pöschel, "Model for collisions in granular gases," Phys. Rev. E **53**, 5382 (1996).
[49]C. Thornton and Z. Ning, "A theoretical model for the stick/bounce behaviour of adhesive, elastic-plastic spheres," Powder Technol. **99**, 154 (1998).
[50]L. Vu-Quoc, X. Zhang, and L. Lesburg, "Contact force–displacement relations for spherical particles accounting for plastic deformation," Int. J. Solids Struct. **38**, 6455 (2001).
[51]L. Vu-Quoc and X. Zhang, "An elasto-plastic contact force-displacement model in the normal direction: Displacement-driven version," Proc. R. Soc. London, Ser. A **455**, 4013 (1999).
[52]X. Zhang and L. Vu-Quoc, "An accurate elasto-plastic frictional tangential force-displacement model for granular flow simulations: Displacement-driven formulation," J. Comput. Phys. **225**, 730 (2007).
[53]S. Schwager, V. Becker, and T. Pöschel, "Coefficient of tangential restitution for visocoelastic spheres," Eur. Phys. J. E: Soft Matter Biol. Phys. **27**, 107 (2008).
[54]C. Thornton, S. J. Cummins, and P. W. Cleary, "An investigation of the comparative behaviour of alternative contact force models during inelastic collisions," Powder Technol. **210**, 189 (2011).
[55]C. Thornton, S. J. Cummins, and P. W. Cleary, "An investigation of the comparative behaviour of alternative contact force models during inelastic collisions," Powder Technol. **233**, 30 (2013).
[56]P. Müller and T. Pöschel, "Oblique impact of frictionless spheres: On the limitations of hard sphere models for granular dynamics," Granular Matter **14**, 115 (2012).
[57]A. Doménech-Carbó, "Analysis of oblique rebound using a redefinition of the coefficient of tangential restitution coefficient," Mech. Res. Commun. **54**, 35 (2013).
[58]A. Doménech-Carbó, "On the tangential restitution problem: Independent friction-restitution modelling," Granular Matter **16**, 573 (2014); , "On the tangential restitution problem: Independent friction-restitution modelling," **16**, 945 (2014).
[59]A. Doménech-Carbó, "On the independence of friction and restitution: An operational approach," Granular Matter **18**, 9 (2016).
[60]A. Doménech-Carbó and C. Doménech-Casasús, "Analysis of microsphere oblique impact with planar surfaces based on the independent friction-restitution approach," J. Aerosol Sci. **140**, 105482 (2020).
[61]A. Doménech-Carbó, "Analysis of rolling friction effects on oblique rebound by redefining tangential restitution and friction," Phys. Fluids **31**, 043302 (2019).
[62]K. Iwashita and M. Oda, "Rolling resistance at contacts in simulation of shear band development by DEM," J. Eng. Mech. **124**, 285 (1998).
[63]A. D. Orlando and H. H. Shen, "Effect of rolling friction on binary collision of spheres," Phys. Fluids **22**, 033304 (2010).
[64]A. Doménech-Carbó and M. T. Doménech-Carbó, "Analysis of two-disc collisions," Eur. J. Phys. **14**, 177 (1993).
[65]K. Voyenli and E. Eriksen, "On the motion of an ice hockey puck," Am. J. Phys. **53**, 1149 (1985).

Published under license by AIP Publishing